PAPER

Optimization of vortex pinning at grain boundaries on *ex-situ* MgB_2 bulks synthesized by spark plasma sintering

To cite this article: Tomoyuki Naito *et al* 2017 *Supercond. Sci. Technol.* **30** 095007

IOP Publishing Superconductor Science and Technology
Supercond. Sci. Technol. **30** (2017) 095007 (8pp) https://doi.org/10.1088/1361-6668/aa6d14

Optimization of vortex pinning at grain boundaries on *ex-situ* MgB_2 bulks synthesized by spark plasma sintering

Tomoyuki Naito, Yuri Endo and Hiroyuki Fujishiro

Faculty of Science and Engineering, Iwate University, Morioka 020-8551, Japan

E-mail: tnaito@iwate-u.ac.jp

Received 25 February 2017, revised 30 March 2017
Accepted for publication 13 April 2017
Published 9 August 2017

Abstract

Grain boundaries are well known to be the predominant pinning centers in MgB_2 superconductors. To study the effects of grain boundaries on the trapped field properties of MgB_2 bulk, we prepared MgB_2 bulks by a spark plasma sintering method using a ball-milled starting powder. The trapped field was maximized for the bulk made from the ball-milled powder with crystallite size, τ, of 27 nm; the highest trapped field, B_T, of 2.3 T achieved at 19.3 K was 1.2 times larger than that of the bulk made from the non ball-milled powder ($\tau = 50$ nm). The degradation of the trapped field for the bulk from finer powder ($\tau = 6$ nm) originated mainly from the lowered T_c. The critical current density, J_c, and the pinning force density, F_p, were also maximized for the bulk from $\tau = 27$ nm. The competition between the increase of the numerical density of grain boundaries and the degradation of superconductivity determined the vortex pinning properties for the MgB_2 bulks with mechanically refined grains. The scaling analysis for the pinning force density suggested that the change in the dimension of the dominant pinning source from 2D (surface) to 0D (point) was induced by grain refining. Although the nanometric impurity particles such as MgB_4, MgO and Mg-B-O were created in the bulk during both ball-milling and spark plasma sintering processes, we considered the point-contact between the refined grains was the predominant point pinning source.

Keywords: trapped field, spark plasma sintering, grain refinement, critical current density, pining force density, MgB_2 bulk

(Some figures may appear in colour only in the online journal)

1. Introduction

A vortex pinning effect realizes a type II superconducting bulk quasi-permanent magnet [1]. A quite compact and strong magnetic field can be used in open space as a conventional permanent magnet. The record-high trapped field of 17.6 T at 26 K was realized at the center of a couple of single-grain Gd-Ba-Cu-O disk-bulks (24.15 mm in diameter and 15 mm in thickness) reinforced by shrinkage fitting of a stainless steel ring [2]. In addition to the promising RE-Ba-Cu-O (RE: rare earth element) bulk magnets, a polycrystalline MgB_2 bulk magnet also offers a strong, homogeneous and highly stable magnetic field [3–16], because of the specific features of MgB_2 such as no weak-linked grains for supercurrent flow [17, 18], a long coherence length [19] and small electromagnetic anisotropy [20]. Although the highest trapped field of 5.4 T at 12 K [9] among MgB_2 bulks is about one third of 17.6 T, the homogeneity and stability of MgB_2 bulk magnets [5, 10, 12] surpasses those of RE-Ba-Cu-O bulk magnets, which is preferable for a magnet used for a compact NMR (nuclear magnetic resonance) system [21]. A target magnetic field of 9.4 T, which corresponds to the NMR frequency of 400 MHz, requires the enhanced B_T to be more than double the current level.

Vortices are well known to be pinned predominantly at the grain boundaries in MgB_2, thus a low-temperature synthesis [22, 23] suppressing the grain growth and/or ball-milled [24] or commercially available nanometer-size [25, 26]

starting powders are often employed to increase the numerical density of grain boundaries. For the MgB_2 tapes sheathed with Fe, which were fabricated by a powder-in-tube method using ball-milled MgB_2 powder via an *ex-situ* route, the J_c increased with decreasing grain size up to a certain grain size, however further finer grains reduced J_c [24]. The J_c increase was attributed to the increased numerical density of the grain boundaries. On the other hand, the J_c decrease for finer grains originated from the fact that the impurities diffusing at the grain surfaces degraded the connectivity between the grains. The similar J_c and B_T characteristics optimized for the grain size were also found in several reports [11, 27, 28]. In contrast, the monotonic increase of J_c with decreasing grain size was observed for MgB_2 being free from the mechanical milling process [26, 29]. Thus, the relationship between the J_c and the grain size is still controversial.

The densification by drawing and a high-pressure synthesis also enhances the grain boundary pinning due to both the increase of numerical density of grain boundaries and the cross-section for supercurrent flow. A spark plasma sintering (SPS) method with a uniaxial pressing is often employed to obtain a dense MgB_2 bulk [30, 31]. The most attractive advantage of this method is quite a short synthesis time, typically ~15 min for MgB_2, which is expected to strongly suppress the grain growth. Actually, almost the same crystallite size was observed between the raw starting and the SPS-processed MgB_2 powders [32]. After the discovery of superconductivity in MgB_2 [33], the B_T of 1 T at 27.5 K was promptly reported for a SPS-processed MgB_2 bulk with 30 mm diameter [3]. Although flux jumps prevented the bulk from trapping higher fields at lower temperatures, this pioneering work demonstrated the potential of MgB_2 bulk magnets. Recently, 2.05 T was trapped by a SPS-processed bulk (30 mm in diameter and 9.7 mm in thickness) at 20 K [15], which was comparable with the B_T of the dense MgB_2 bulks prepared by the conventional high-pressing methods such as hot isostatic pressing (HIP) and hot pressing (HP). We have developed the strong *in-situ* MgB_2 bulk magnets trapping 3–5 T class by densification using the HIP [8] and infiltration [16] methods and the doping of the impurities such as Ti [12] and SiC [34]. To further realize the higher trapped field for the MgB_2 bulk, in this paper, we studied the effects of grain refining and the SPS process on the trapped field properties of *ex-situ* SPS-processed MgB_2 bulks using various ball-milled powders.

2. Experimental procedure

MgB_2 bulks were fabricated by an *ex-situ* SPS method (LABOX-110, SINTER LAND Inc., Ltd.) using a commercially available MgB_2 powder (99% in purity, Furuuchi Chemical Co.). As-manufactured MgB_2 powder was pulverized by a planetary ball-milling device (PM100, Retsch GmbH). We prepared three kinds of starting powders with different crystallite size, τ, by controlling the rotation speed (0−600 rpm) for a constant duration of 12 h in the ball-milling process, in which the stainless steel (SUS304) balls (10 mm in diameter) and container were used. Each starting powder was poured into a set of graphite die and punches lined with graphite paper, and pelletized preliminarily under a uniaxial stress of 10 MPa. This was sintered in the SPS apparatus in a vacuum of 20–100 Pa for 5–15 min at 950 °C–1050 °C under the uniaxial pressure of 50 MPa; the temperature was monitored on the surface of the graphite die using a radiation thermometer. The filling factors, f, of the bulks, which were the ratio of the measured to theoretical mass densities, were typically ~90%. The constituent phase and structure of the MgB_2 samples were evaluated by x-ray diffraction using Cu-Kα radiation (with a wavelength of 0.154 nm) operated with an acceleration voltage of 30 kV and electron current of 30 mA.

An MgB_2 bulk was magnetized by field cooling (FC) in the following procedure. It was cooled down to a target temperature in a magnetic field of 5 T parallel to the thickness direction using a 10 T cryogen-free superconducting magnet (JMTD-10T100, Japan Superconductor Technology, Inc.) using a G-M type cryo-cooler. After the applied magnetic field was ramped down to 0 T at a rate of 0.022-0.22 T min^{-1}, the trapped field was measured by a cryogenic Hall sensor (HP-VVP, AREPOC r.s.o.) mounted on the center of the bulk surface using GE7031 varnish. The temperature of the bulk was monitored by a Cernox thermometer which was adhered beside the Hall sensor on the bulk surface. After the FC magnetization experiments, the superconducting properties such as the critical temperature, T_c, and the critical current density, J_c, were evaluated using a small piece cut from the bulk. Magnetization, M, was measured as a function of temperature and magnetic field using a commercial SQUID magnetometer (MPMS-XL, Quantum Design Inc.). J_c was estimated from the magnetic hysteresis using the extended Bean model [35, 36], $J_c = 20\Delta M/a(1 - a/3b)$, where ΔM is the width of the hysteresis, and a and b ($a < b$) are the cross-sectional dimensions of the sample perpendicular to the applied magnetic field. Microstructure and chemical composition were analyzed by a electron probe micro analyzer with a field emission electron gun (FE-EPMA; JXA-8100/8200, JEOL Ltd.) and a scanning electron microscopy (SEM; JSM-7001F, JEOL Ltd.) coupled with electron backscatter diffraction (EBSD; NordlysNano, Oxford Instruments plc).

3. Results and discussion

3.1. Characterization of the SPS-processed MgB_2 bulks

Figure 1(a) shows the powder X-ray diffraction patterns of the as-produced and ball-milled (BM) powders. The as-produced (non-BM) powder was confirmed to be a single phase of MgB_2. On the other hand, the MgB_4 impurity phase appeared for the ball-milled powders in addition to the main phase of MgB_2. The diffraction peaks broadened noticeably owing to the ball-milling. The crystallite size, τ, of the powder was

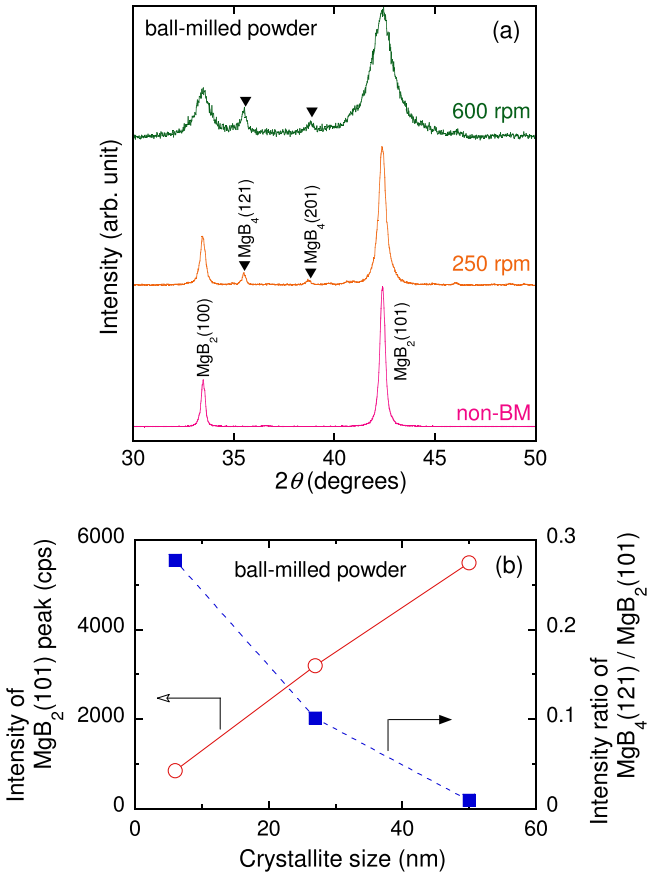

Figure 1. (a) Powder x-ray diffraction patterns of the as-produced and ball-milled powders. (b) The raw intensity of $MgB_2(101)$ peak (left axis) and the intensity ratio of the $MgB_4(121)$ to $MgB_2(101)$ peaks (right axis) as a function of the crystallite size, τ.

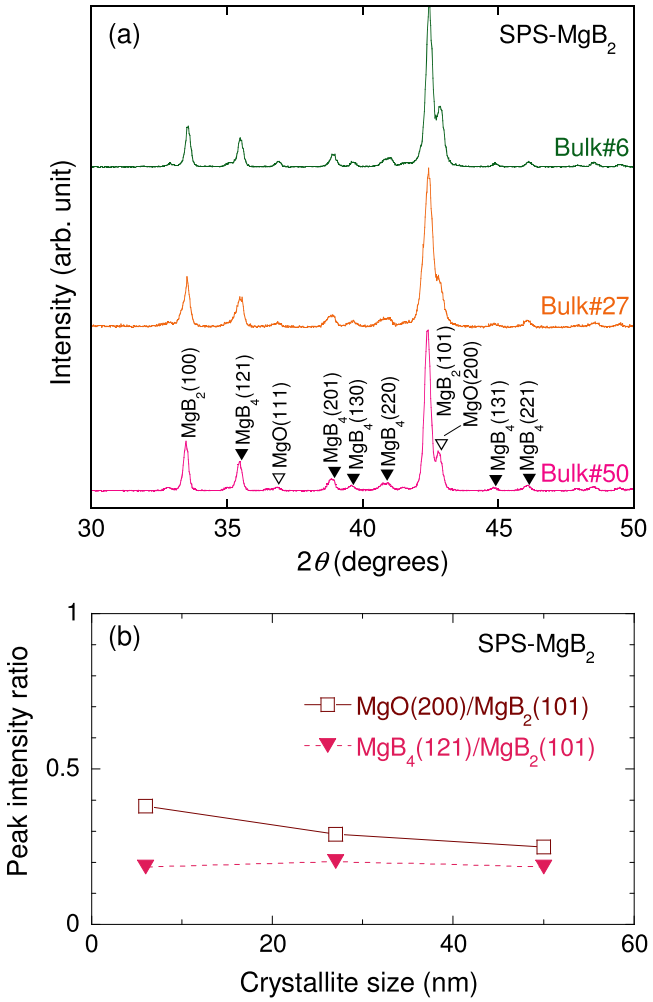

Figure 2. (a) X-ray diffraction patterns of three SPS-processed MgB_2 bulks. (b) The peak intensity ratios of $MgO(200)/MgB_2(101)$ and of $MgB_4(121)/MgB_2(101)$ as a function of the crystallite size, τ.

estimated by the following Scherrer's relation [37],

$$\tau = \frac{K\lambda}{\beta \cos\vartheta}, \quad (1)$$

where K is the shape factor, generally $\sim$0.9, λ the wavelength of the Cu-Kα radiation, β the full width at half maximum (FWHM) of the diffraction peak, and ϑ the Bragg angle. The τ value of 50 nm estimated for the non-BM powder was reduced to 27 nm and 6 nm by ball-milling with rotation speeds of 250 rpm and 600 rpm, respectively. Figure 1(b) shows the raw intensity of the $MgB_2(101)$ peak (left axis) and the intensity ratio of the $MgB_4(121)$ to $MgB_2(101)$ peaks (right axis) as a function of τ. The monotonic decrease of the $MgB_2(101)$ peak intensity suggests the degradation of the crystallinity by the mechanical shock. The increase of the relative amount of MgB_4 indicates that a decomposition reaction, $2MgB_2 \rightarrow Mg + MgB_4$, was promoted by the ball milling. No detectable XRD peak relating to the residual Mg indicates the existence of amorphized Mg and/or MgO below the detection limit of XRD.

Figure 2(a) shows the x-ray diffraction patterns of the MgB_2 bulks made from the starting powders with different τ (50 nm, 27 nm, 6 nm). They were named Bulk#50, Bulk#27, and Bulk#6, respectively. Both MgB_4 and MgO impurity phases appeared in all the MgB_2 bulks. That there was no MgB_4 in the as-produced (non-BM) MgB_2 powder suggests that MgB_4 in the bulks was created via the decomposition reaction ($2MgB_2 \rightarrow Mg + MgB_4$) during the SPS process. This is consistent with the decomposition temperature of MgB_2, which was reported to be 897 °C–1071 °C [31, 38]. On the other hand, MgO was created from dissolved Mg vapor which reacted with the oxygen absorbed on the surface of grain and/or the residual oxygen in the SPS apparatus. As shown in figure 2(b), the peak intensity ratio of $MgO(200)/MgB_2(101)$ slightly increased with decreasing τ, and that of $MgB_4(121)/MgB_2(101)$ is almost independent of the τ value. These results mean that almost the same amount of MgB_4 and MgO impurities should be contained in three bulks, despite each starting powder having different amounts of them.

Figure 3 shows the temperature dependence of the normalized magnetization at $\mu_0 H = 0.4$ mT after zero-field cooling for the MgB_2 bulks. All the bulks represented a sharp superconducting transition. The critical temperatures, T_c, defined at the mid-point were 37.9 K, 37.4 K, and 35.0 K for Bulk#50, Bulk#27, and Bulk#6, respectively. The

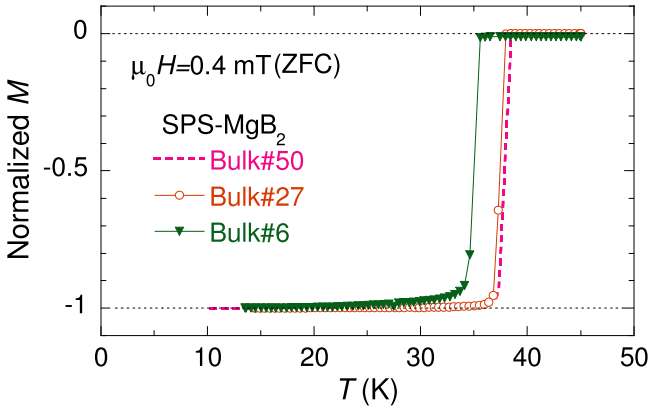

Figure 3. Temperature dependence of the normalized magnetization in a magnetic field of 0.4 mT after zero-field cooling for three SPS-processed MgB_2 bulks.

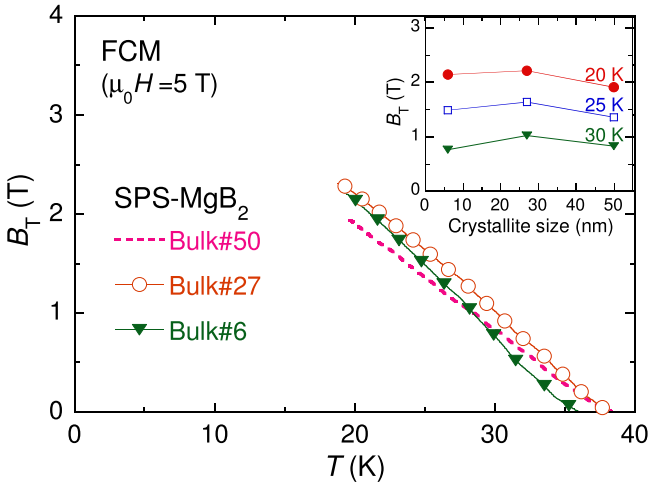

Figure 4. Temperature dependence of the trapped field by the FCM under a magnetic field of 5 T for three SPS-processed MgB_2 bulks. Inset shows the trapped field at $T = 20$, 25 and 30 K as a function of the crystallite size, τ.

suppression of T_c probably originated from the degraded crystallinity of the starting MgB_2 powder.

3.2. Magnetic properties and microstructure of the SPS-processed MgB_2 bulks

Figure 4 shows the temperature dependence of the trapped magnetic field, $B_T(T)$, for the MgB_2 bulks. The B_T increased with decreasing temperature for all the bulks due to the J_c increase by cooling. The B_T of 1.9 T at 20 K for Bulk#50 was comparable with the B_T of 2.05 T obtained for the larger SPS-processed MgB_2 bulk 30 mm in diameter [15]. The $B_T(T)$ curve of Bulk#27 was pushed up entirely with respect to that of Bulk#50, and the highest B_T was 2.3 T at 19.3 K. The B_T of Bulk#6 was smaller than that of Bulk#50 from 36 K down to 28 K because of low T_c. However, it started to increase steeply around 30 K, exceeded the B_T of Bulk#50, and then approached the B_T of Bulk#27. This indicates that the 'positive' effect of the increase of pinning centers exceeds the 'negative' effect of the lowering T_c by the ball-milling below 30 K. As shown in the inset of figure 4, the B_T was obviously maximized at $\tau = 27$ nm (for Bulk#27) at $T = 20$ K, 25 K, and 30 K.

Figure 5(a) shows the magnetic field dependence of the critical current density, $J_c(\mu_0 H)$, at 10 K and 20 K for the MgB_2 bulks. The $J_c(\mu_0 H)$ decreased monotonically with increasing magnetic field for all the MgB_2 bulks, which is common behavior for MgB_2. The $J_c(\mu_0 H)$ for Bulk#27 was evidently enhanced by the grain refining. In particular, the irreversibility field, $\mu_0 H_{irr}$, was shifted from 4.2 T for Bulk#50 to about 5 T for Bulk#27 at 20 K, where $\mu_0 H_{irr}$ was defined by a magnetic field at $J_c = 10$ A cm^{-2}. On the other hand, a small enhancement of $J_c(\mu_0 H)$ was observed for Bulk#6 with respect to the $J_c(\mu_0 H)$ for Bulk#50. The J_c at $\mu_0 H = 0$ T and 3 T are plotted as a function of the crystallite size, τ, for various temperatures in figures 5(b) and (c), respectively. J_c versus τ shows a peak at $\tau = 27$ nm (for Bulk#27) for both 0 T and 3 T, similarly to the B_T versus τ as shown in the inset of figure 4.

To understand the obtained B_T and J_c characteristics, we considered the pinning force density, F_p. Figure 6(a) shows the magnetic field dependence of the pinning force density, $F_p(\mu_0 H)$, at 20 K for the MgB_2 bulks. The grain refining evidently enhanced the $F_p(\mu_0 H)$. Bulk#27 took the maximum, F_p^{max}, of 1.6 GN m^{-3} at 1 T, which was 1.7 times larger than the F_p^{max} of 0.92 GN m^{-3} at 0.8 T for Bulk#50. Somewhat enhanced F_p^{max} of 1.1 GN m^{-3} at 1 T was observed for Bulk#6. The dominant pinning mechanism in the present bulks was estimated by two scaling functions [39, 40] as follows. As shown in figure 6(b), the conventional scaling function [39], $f_p(=F_p/F_p^{max}) \propto h_i^p(1-h_i)^q$, reproduced the experimental f_p with $p = 0.74$ and $q = 2.7$ for Bulk#50, $p = 0.96$ and $q = 2.8$ for Bulk#27 and $p = 0.94$ and $q = 3.4$ for Bulk#6. Here h_i is the normalized field, $h_i = \mu_0 H/\mu_0 H_{irr}$ and the exponents p and q are characteristics for the dominant pinning mechanism. Theoretical prediction of $p = 0.5$ and $q = 2$ for the normal surface pinning and $p = 1$ and $q = 2$ for the normal core point pinning suggests the change in the dominant pinning mechanism from the normal surfaces to the normal cores by grain refining, in spite of somewhat deviated p and q values. The large $q(>2)$ values were often found for various materials such as $YBa_2Cu_3O_{7-\delta}$ [41], Nb_3Sn [42], and other MgB_2 [29]. Since the theoretical $q = 2$ is for a homogeneous isotropic superconductor, Wördenweber took the Gaussian distribution of a specific critical field in channels for the vortex motion as the inhomogeneity into account for the $F_p(\mu_0 H)$ calculation, and then obtained the simulated q values larger than 2 [43]. On the other hand, Eisterer demonstrated that the anisotropy changed substantially the field dependence of F_p and the theoretical Kramer plot [40], which possibly changes the conventional theoretical parameters of p and q. Therefore, the inhomogeneity of the present MgB_2 bulks, as found in figure 7, and the anisotropic nature of MgB_2 probably offered the large q value of ~3. To solve the problems in the conventional scaling, Eisterer proposed a new F_p-scaling procedure [40] by taking the anisotropy parameter γ and the percolation threshold p_{sh} into account, where p_{sh} is defined as the minimum fraction of the superconducting region for a continuous

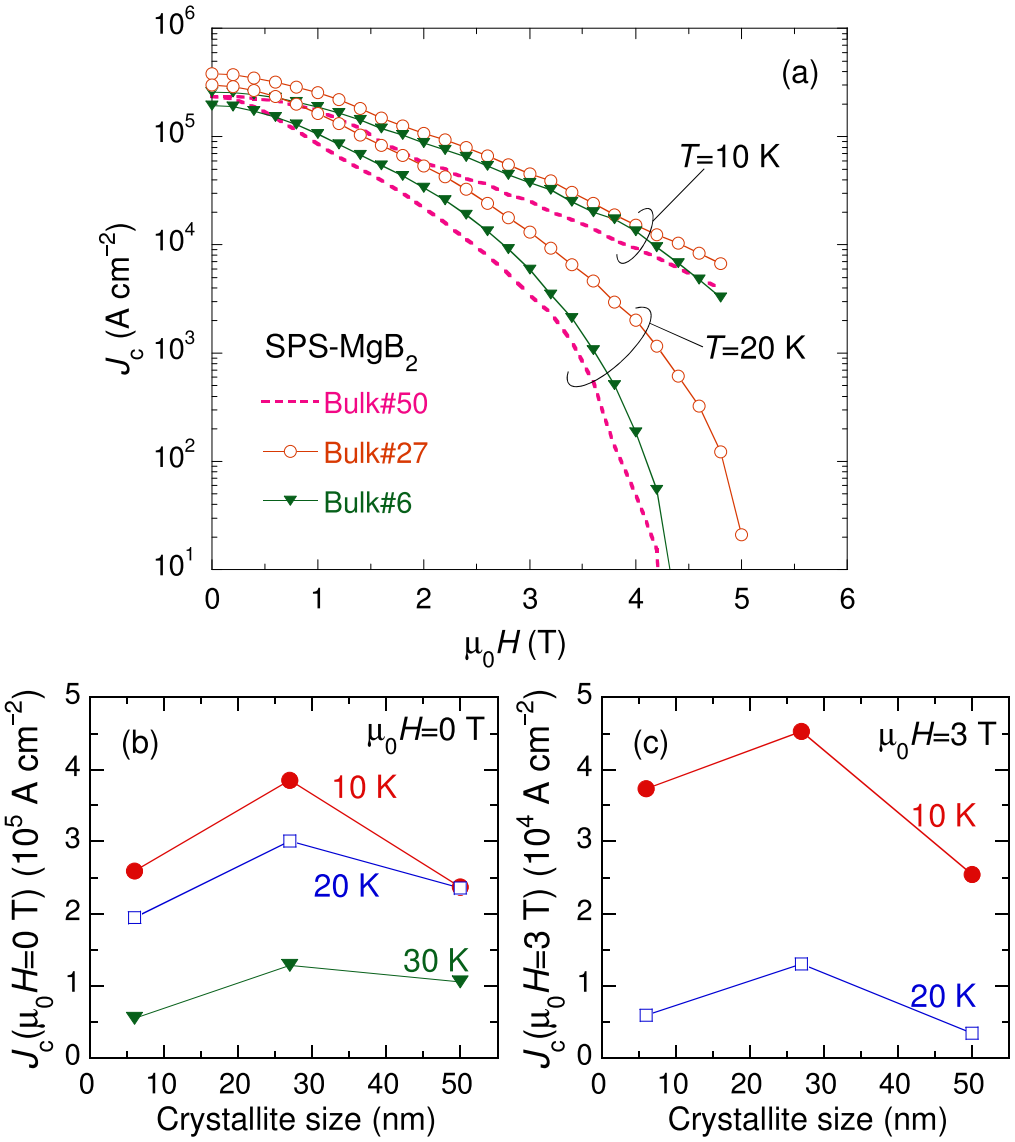

Figure 5. (a) Magnetic-field dependence of the critical current density, $J_c(\mu_0 H)$, at $T = 10$ and 20 K for three SPS-processed MgB_2 bulks. (b) and (c), respectively, show the J_c at $\mu_0 H = 0$ and 3 T for the indicated temperatures as a function of the crystallite size, τ.

supercurrent path. In this scaling, a reduced peak-field, $h_{n,peak}$, at the f_p^{max} in the f_p versus h_n plot, as shown in figure 6(c), determines directly the dominant pinning center. Here, the $h_n(=\mu_0 H/\mu_0 H_n)$ is the normalized field and $\mu_0 H_n$ is defined as the magnetic field at which F_p drops to half of F_p^{max} at magnetic fields above the peak magnetic field. The $h_{n,peak}$ values of 0.35, 0.43 and 0.43 obtained for Bulk#50, Bulk#27 and Bulk#6, respectively, strongly support that the surface pinning for the non-BM bulk changes to the point pinning centers for the grain-refined bulks, by referring to the theoretically predicted $h_{n,peak}$ values with $\gamma = 4$ and $p_{sh} = 0.25$ for the typical pinning sources with the combination of p and q values in the following; (1) $h_{n,peak} = 0.34$ for normal surface pinning ($p = 1/2$, $q = 2$), (2) $h_{n,peak} = 0.47$ for normal point pinning ($p = 1$, $q = 2$), (3) $h_{n,peak} = 0.56$ for superconducting volume pinning ($p = 1$, $q = 1$), (4) $h_{n,peak} = 0.62$ for superconducting surface pinning ($p = 3/2$, $q = 1$) and (5) $h_{n,peak} = 0.65$ for superconducting point pinning ($p = 2$, $q = 1$). The two scaling results suggest strongly the predominant point pinning for the bulks made from the BM powder.

Let us consider the point pinning source introduced by grain refining and SPS processes from the microstructural analysis. Figure 7 shows the backscattered electron (compositional contrast) images for three MgB_2 bulks. A dark gray spot in the light gray matrix increased and dispersed finely in the order of Bulk#50, Bulk#27, Bulk#6. The typical chemical compositions at the indicated positions were examined quantitatively by FE-EPMA, which were summarized in table 1. The chemical compositions of the light gray and of dark gray regions, respectively, were MgB_y ($y = 2.4$–2.7) and MgB_y ($y = 2.8$–4.2) with a small amount of oxygen. This suggests that the fine MgB_y ($y > 2$) and MgO particles dispersed in the MgB_2 matrix (light gray region) and that the MgB_4 dominates in the dark gray regions. Bright regions contained five to ten times as much oxygen compared to the

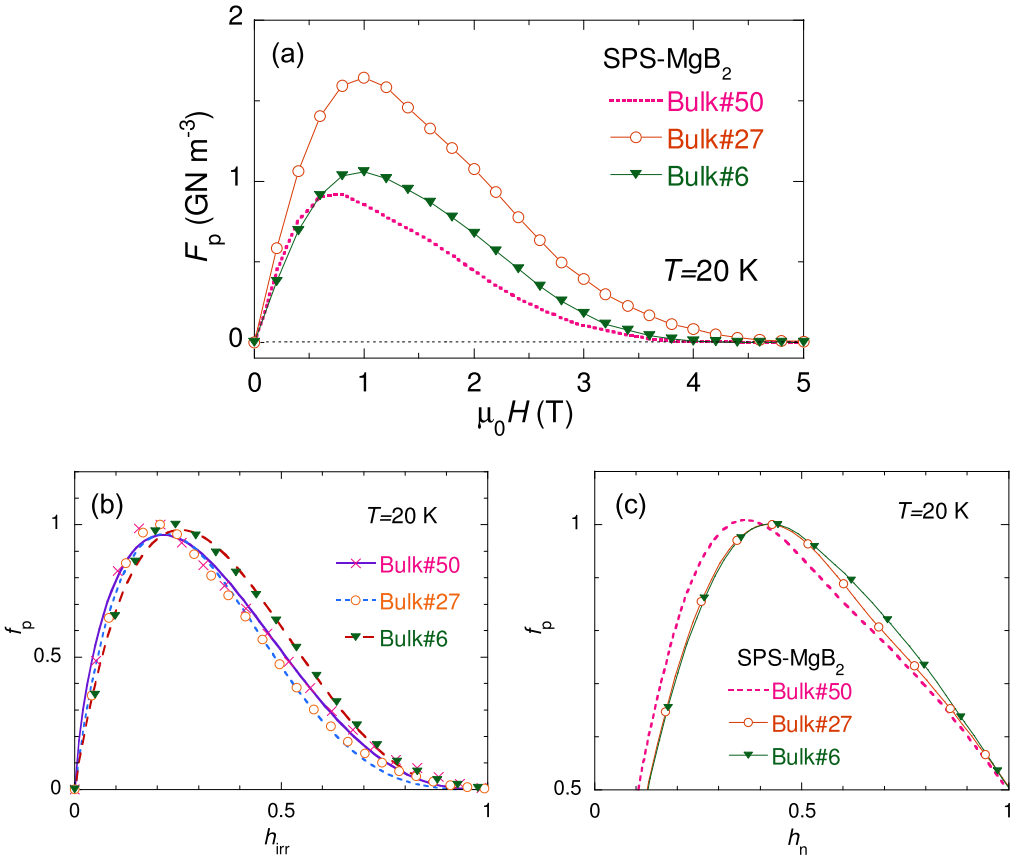

Figure 6. (a) Magnetic-field dependence of the pinning force density, $F_p(\mu_0 H)$, at $T = 20$ K for three SPS-processed MgB_2 bulks; (b) and (c), respectively, show the reduced pinning force densities, f_p, versus the reduced field h_{irr} and h_n at 20 K.

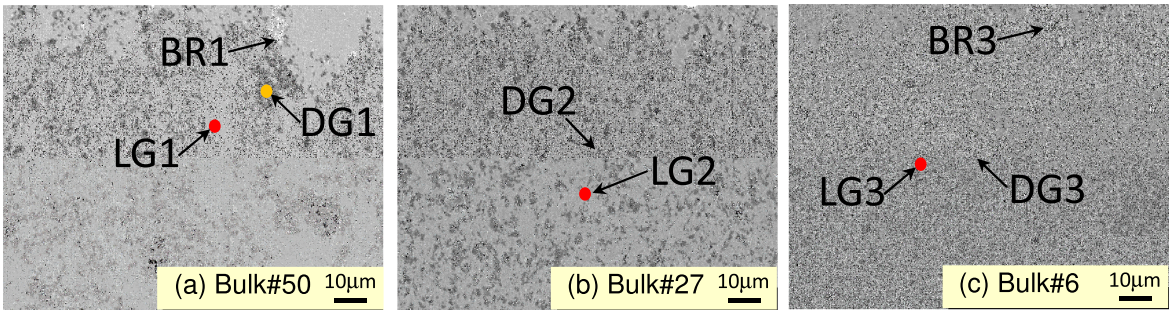

Figure 7. Backscattered electron (compositional contrast) images for three SPS-processed MgB_2 bulks.

Table 1. Typical chemical composition ratio of three SPS-processed MgB_2 bulks. LG, DG and BR mean light gray, dark gray and bright regions, respectively (see text and figure 7).

	Bulk#50			Bulk#27		Bulk#6		
	LG1	DG1	BR1	LG1	DG1	LG3	DG3	BR3
Mg	1	1	1	1	1	1	1	1
B	2.50	4.23	2.14	2.41	2.82	2.69	3.52	3.41
O	0.06	0.07	0.54	0.10	0.11	0.22	0.07	0.44

amount of both gray regions. These are probably Mg-B-O compounds as pointed out by previous papers [44–47].

Figure 8 shows the electron backscattered diffraction (EBSD) images for three bulks. The mosaic pattern demonstrates the randomly oriented MgB_2 grains. The grain size apparently reduced, and concurrently an unanalyzed 'black' area increased, in the order of Bulk#50, Bulk#27, Bulk#6. The unanalyzed area probably corresponds to the voids and grains finer than the resolution limit of 50 nm for the EBSD device and/or an amorphous phase; both result in difficulties in Kikuchi pattern indexing. Considering both the XRD patterns indexed mainly by MgB_2 and the degradation of T_c, the ball-milling does not offer amorphous MgB_2 but instead offers the nanometric deformed MgB_2 crystal for both Bulk#27 and Bulk#6. The EBSD results confirm that Bulk#6 has the largest numerical density of the grain boundary among the present bulks, however the trapped field is maximized for Bulk#27. This originated from the competition between two effects given by ball-milling, i.e. the

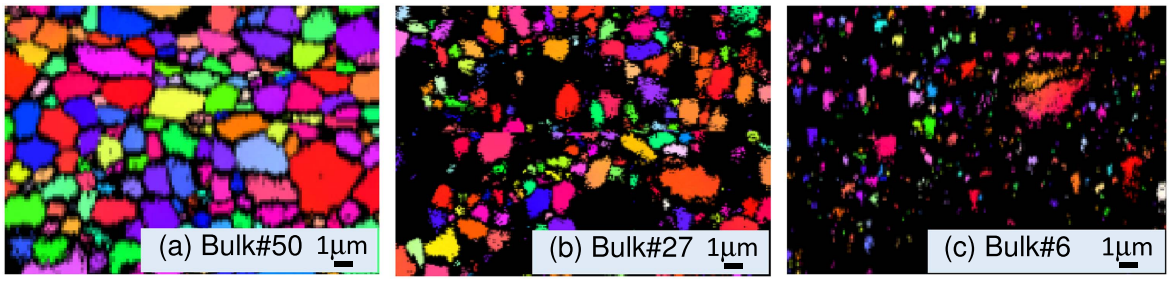

Figure 8. Electron backscattered diffraction (EBSD) images for three SPS-processed MgB_2 bulks.

increase of the pinning centers and the deterioration of the superconductivity of the MgB_2 matrix due to the deformation of the MgB_2 crystals, which degrades the elemental pinning force. Since the contact cross-section between the grains becomes small with decreasing grain size, the nature of the grain boundaries should be changed from a planar to a point-contact, that is, the 2D (correlated) to 0D (point-like) pinning centers by grain refining. This explains the characteristics of pinning force density shown in figure 6. As found in figure 7, the micrometric impurity-rich regions are obviously reduced by the ball-milling and SPS processes. They are too large to be the effective pinning centers, considering the vortex-core size, $\sim 2\xi$, where $\xi \sim 10$ nm was reported for MgB_2 [48]. The XRD results shown in figure 2 suggest that the amount of impurities, approximately the product of their number and volume (size), are comparable for three bulks. That there is almost the same FWHM of $MgB_4(121)$ peaks and the fact that MgO was created from the dissolved Mg vapor and residual oxygen suggest the comparable size of both impurities for three bulks. The Mg-B-O might be a nanometer-size $Mg(B, O)_2$ precipitate [45]. Actually, the fine MgB_y ($y > 2$), MgO and Mg-B-O particles must act as 'point' pinning centers [44–47]. Consequently, they seem not to play the principal role in the 'dimensional change' of the pinning mechanism. The similar grain size dependent B_T properties were already reported [11], in which the authors pointed out that the enhancement of B_T was due to the increase of the grain boundary density and electron scattering. Contrary to the present results, both J_c and F_p increased monotonically with a reduction in grain size for MgB_2 made from the raw starting powder without mechanical milling [26, 29]. This suggests that the use of such fine starting powder, which probably contains clean grain boundaries, further improved the trapped field properties of the *ex-situ* MgB_2 bulks.

4. Summary

We have studied the trapped field properties of MgB_2 bulks made from the as-produced and ball-milled starting MgB_2 powders with different crystallite size, τ, 50, 27 and 6 nm, using the spark plasma sintering (SPS) method. The obtained important results are listed below.

(i) A bulk made from the $\tau = 27$ nm powder offered the highest B_T of 2.3 T at 19.3 K, which was 1.2 times larger than the B_T of 1.9 T for a bulk made from the $\tau = 50$ nm powder. The vortex pinning characteristics including the critical current density, J_c, and the pinning force density, F_p, were also maximized for the $\tau = 27$ nm bulk. The optimal grain size was determined apparently by the balance of the increase of the pinning centers with the degradation of superconductivity.

(ii) The dominant pinning source changed from the surface (two-dimensional) to the point (zero-dimensional) pinning by the grain refining from the scaling analysis for the pinning force density. We proposed that the grain boundaries possibly acted as the point-like pinning centers when a contact cross-section of MgB_2 grains became smaller than a certain threshold value.

(iii) Both ball-milling and SPS processes created the MgB_4, MgO and Mg-B-O impurities as the nanometric particles. These also acted as the point pinning centers, but did not play the principal role in the dimensional change of the dominant pinning source.

Acknowledgments

We would like to thank Drs K Nonaka and T Murakami of Iwate University for their help in the microstructure analysis using FE-EPMA and SEM-EBSD apparatuses. This work was partly supported by JSPS KAKENHI Grant Numbers JP15K04718, JP15K04646.

References

[1] Gotoh S, Murakami M, Fujimoto H and Koshizuka N 1992 *J. Appl. Phys.* **72** 2404–10
[2] Durrell J H *et al* 2014 *Supercond. Sci. Technol.* **27** 082001
[3] Murakami M and Yoo S I 2003 (in Japanese) http://moniko.s26.xrea.com/shinbunhappyou/MgB2.htm
[4] Viznichenko R V, Kordyuk A A, Fuchs G, Nenkov K, Müller K H, Prikhna T A and Gawalek W 2003 *Appl. Phys. Lett.* **83** 4360–2
[5] Naito T, Sasaki T and Fujishiro H 2012 *IEEE Trans. Appl. Supercond.* **22** 4401703
[6] Naito T, Sasaki T and Fujishiro H 2012 *Supercond. Sci. Technol.* **25** 095012
[7] Durrell J H, Dancer C E J, Dennis A, Shi Y, Xu Z, Campbell A M, Babu N H, Todd R I, Grovenor C R M and Cardwell D A 2012 *Supercond. Sci. Technol.* **25** 112002

[8] Sasaki T, Naito T and Fujishiro H 2013 *Phys. Procedia* **45** 93–6
[9] Fuchs G, Häßler W, Nenkov K, Scheiter J, Perner O, Handstein A, Kanai T, Schultz L and Holzapfel B 2013 *Supercond. Sci. Technol.* **26** 122002
[10] Yamamoto A, Ishihara A, Tomita M and Kishio K 2014 *Appl. Phys. Lett.* **105** 032601
[11] Sugino S, Yamamoto A, Shimoyama J and Kishio K 2015 *Supercond. Sci. Technol.* **28** 055016
[12] Naito T, Yoshida T and Fujishiro H 2015 *Supercond. Sci. Technol.* **28** 095009
[13] Mochizuki H, Fujishiro H, Naito T, Albisetti A F and Giunchi G 2015 *Supercond. Sci. Technol.* **28** 105004
[14] Bhagurkar A G, Yamamoto A, Anguilano L, Dennis A R, Durrell J H, Babu N H and Cardwell D A 2016 *Supercond. Sci. Technol.* **29** 035008
[15] Berger K, Koblischka M R, Douine B, Noudem J, Bernstein P, Hauet T and Lévêque J 2016 *IEEE Trans. Appl. Supercond.* **26** 6801005
[16] Naito T, Ogino A and Fujishiro H 2016 *Supercond. Sci. Technol.* **29** 115003
[17] Kambara M, Babu N H, Sadki E S, Cooper J R, Minami H, Cardwell D A, Campbell A M and Inoue I H 2001 *Supercond. Sci. Technol.* **14** L5–7
[18] Larbalestier D C *et al* 2001 *Nature* **410** 186–9
[19] Finnemore D K, Ostenson J E, Bud'ko S L, Lapertot G and Canfield P C 2001 *Phys. Rev. Lett.* **86** 2420–2
[20] Bud'ko S L and Canfield P C 2002 *Phys. Rev.* B **65** 212501
[21] Nakamura T, Tamada D, Yanagi Y, Itoh Y, Nemoto T, Utumi H and Kose K 2015 *J. Magn. Reson.* **259** 68–75
[22] Kumakura H, Kitaguchi H, Matsumoto A and Hatakeyama H 2004 *Appl. Phys. Lett.* **84** 3669–71
[23] Yamamoto A, Shimoyama J, Ueda S, Katsura Y, Horii S and Kishio K 2005 *Supercond. Sci. Technol.* **18** 116
[24] Flükiger R, Suo H, Musolino N, Beneduce C, Toulemonde P and Lezza P 2003 *Physica* C **385** 286–305
[25] Chen S K, Yates K A, Blamire M G and MacManus-Driscoll J L 2005 *Supercond. Sci. Technol.* **18** 1473
[26] Katsura Y, Yamamoto A, Ueda S, Iwayama I, Horii S, Shimoyama J and Kishio K 2006 *J. Phys.: Conf. Ser.* **43** 119
[27] Dancer C E J, Prabhakaran D, Crossley A, Todd R I and Grovenor C R M 2010 *Supercond. Sci. Technol.* **23** 065015
[28] Vignolo M *et al* 2008 *IEEE Trans. Appl. Supercond.* **18** 1175–8
[29] Martínez E, Mikheenko P, Martínez-López M, Millán A, Bevan A and Abell J S 2007 *Phys. Rev.* B **75** 134515
[30] Lee S Y, Yoo S I, Kim Y W, Hwang N M and Kim D Y 2003 *J. Am. Ceram. Soc.* **86** 1800–2
[31] Schmidt J, Schnelle W, Grin Y and Kniep R 2003 *Solid State Sci.* **5** 535–9
[32] Aldica G, Batalu D, Popa S, Ivan I, Nita P, Sakka Y, Vasylkiv O, Miu L, Pasuk I and Badica P 2012 *Physica* C **477** 43–50
[33] Nagamatsu J, Nakagawa N, Muranaka T, Zenitani Y and Akimitsu J 2001 *Nature* **410** 63–4
[34] Naito T *et al* private communication
[35] Bean C P 1962 *Phys. Rev. Lett.* **8** 250–3
[36] Gyorgy E M, van Dover R B, Jackson K A, Schneemeyer L F and Waszczak J V 1989 *Appl. Phys. Lett.* **55** 283–5
[37] Cullity B 1956 *Elements of X-ray Diffraction* (Reading, MA: Addison-Wesley)
[38] Guo Y, Zhang W, Yang D and Yao R L 2012 *J. Am. Ceram. Soc.* **95** 754–9
[39] Dew-Hughes D 1974 *Phil. Mag.* **30** 293–305
[40] Eisterer M 2008 *Phys. Rev.* B **77** 144524
[41] Li J, Boer F D, Roeland L, Menken M, Kadowaki K, Menovsky A and Franse J 1990 *Physica* C **169** 81–6
[42] Cheggour N and Hampshire D P 2002 *Cryogenics* **42** 299–309
[43] Wördenweber R 1992 *Phys. Rev.* B **46** 3076–83
[44] Zhu Y, Wu L, Volkov V, Li Q, Gu G, Moodenbaugh A, Malac M, Suenaga M and Tranquada J 2001 *Physica* C **356** 239–53
[45] Liao X Z, Serquis A, Zhu Y T, Huang J Y, Civale L, Peterson D E, Mueller F M and Xu H F 2003 *J. Appl. Phys.* **93** 6208–15
[46] Prikhna T *et al* 2015 *J. Supercond. Nov. Magn.* **28** 525–30
[47] Naito T, Yoshida T, Mochizuki H, Fujishiro H, Basu R and Szpunar J A 2016 *IEEE Trans. Appl. Supercond.* **26** 6800805
[48] Buzea C and Yamashita T 2001 *Supercond. Sci. Technol.* **14** R115